RSC Advances

ROYAL SOCIETY OF CHEMISTRY

www.rsc.org/advances

Dehydrochlorination mechanism of γ-hexachlorocyclohexane degraded by dehydrochlorinase LinA from *Sphingomonas paucimobilis* UT26

Xiaowen Tang, Ruiming Zhang, Qingzhu Zhang*, Wenxing Wang

Environment Research Institute, Shandong University,

Jinan 250100, P. R. China

Keywords

γ-Hexachlorocyclohexane, Dehydrochlorinase LinA, Degradation mechanism, Quantum mechanics/molecular mechanics, Boltzmann-weighted average

*Corresponding authors. E-mail: zqz@sdu.edu.cn,

Fax: 86-531-8836 1990

Abstract

This study investigated the aerobic degradation mechanism from γ-HCH to 1,3,4,6-TCDN catabolized by dehydrochlorinase LinA from *Sphingomonas paucimobilis* UT26. The enzymatic step was studied by a combined quantum mechanics/molecular mechanics (QM/MM) computation and the nonenzymatic step was investigated by the DFT method. There are three elementary steps involved in the degradation process. Two discontinuous dehydrochlorination reactions with the Boltzmann-weighted average potential barriers of 16.2 and 17.3 kcal/mol are connected by a conformational transition with a barrier of 11.1 kcal/mol. The electrostatic influence analysis of fourteen key residues surrounding the active site has been carried out. The study reveals that Phe68 facilitates the dehydrochlorination of γ-HCH, whereas Leu21 and Cys71 suppress it. The mutation studies for improving the degradation efficiency of LinA can focus on mutating the amino acids of Leu21 and Cys71.

1. Introduction

Hexachlorocyclohexane (HCH) is an organochlorine compound with several stable isomers. Among all the isomers, only the γ isomer (γ-hexachlorocyclohexane, γ-HCH) has insecticidal properties and has been widely used as broad-spectrum insecticide to control a wide range of agricultural, horticultural, and public health pests (*1-3*). Two kinds of γ-HCH products, technical

HCH (the content of γ-HCH is 10-15%) and lindane (purified γ-HCH), have been applied and about 600,000 tons were released into environment between 1940s and 1990s (*4-5*). Due to its non-target toxicity and environmental persistence, HCH was included in the list of persistent organic pollutants (POPs) according to the Stockholm convention in 2009 (*6*), and has been prohibited in most countries. However, lindane is still used in some developing countries for its high efficiency and low cost (*3,7*). Therefore, the HCH contamination, especially γ-HCH contamination, is continuously a serious threat to the environment.

Microbial degradation of γ-HCH can proceed under either anaerobic or aerobic condition (*8-10*). Chlorobenzene and benzene will be accumulated when γ-HCH is degraded under the anaerobic condition. The biochemical pathways for anaerobic degradation of γ-HCH are available, but unfortunately the specific genes and enzymes involved in the anaerobic degradation have not been identified yet (*4*). In contrast, γ-HCH can be degraded completely into nontoxic molecules under the aerobic condition. Researches about the aerobic degradation of γ-HCH are numerous and several HCH-degrading aerobes have been described in details (*1,11-15*). Most of them belong to the family of *Sphingomonadaceae* (*16*). They contain a set of genes called *lin* genes, which can encode HCH degradation enzymes. The aerobic degradation pathway of γ-HCH is devoted by various enzymes, among which the HCH dehydrochlorinase (LinA) from *Sphingobium japonicum* UT26 is considered to be significant because it catalyzes the initial step of the γ-HCH aerobic degradation (*17-18*).

LinA catalyzes the dehydrochlorination of γ-HCH to generate an observed intermediate γ-pentachlorocyclohexene (γ-PCCH), which is transformed to a putative product 1,3,4,6-tetrachloro-1,4-cyclohexadiene (1,3,4,6-TCDN) through another dehydrochlorination step (*19*). During the LinA-catalyzed degradation process, the substrate is released from the enzyme after the first dehydrochlorination reaction and rebinds to the active site of LinA when undergoing the subsequent dehydrochlorination reaction (*17*). Crystal structure studies revealed that a catalytic dyad formed by His73 and Asp25 is located in the active site of LinA (*17*-*18*). During the enzymatic dehydrochlorination reaction, His73 of LinA acts as a general base to grab the proton of substrate, generating a positively charged His73 residue which is stabilized though its interaction with Asp25 (*20*). It is generally considered that the leaving hydrogen and chlorine in the LinA-catalyzed dehydrochlorination reaction should be axial, adjacent and in antiparallel position (*21*). Hence, LinA exclusively catalyzes the dehydrochlorination reaction of the substrates containing at least one adjacent *trans*-diaxial H/Cl pair. The biotransformation mechanism from γ-HCH to 1,3,4,6-TCDN is exhibited in Scheme 1A. The hydrogen atom bonded to C^1 and chlorine atom bonded to C^2, composing an adjacent *trans*-diaxial H/Cl pair (H^1/Cl^2), are removed in the dehydrochlorination reaction of γ-HCH by LinA. Enzymatic dehydrochlorination of the newly generated intermediate (γ-PCCH) must proceed through the elimination of H^4/Cl^5 pair during the transformation from γ-PCCH to 1,3,4,6-TCDN. However, neither of them in γ-PCCH is situated on axial orientation, implying that γ-PCCH is unable to transform to 1,3,4,6-TCDN by enzymatic

dehydrochlorination directly. Actually, the formation of 1,3,4,6-TCDN can accomplish through the LinA-catalyzed dehydrochlorination of a PCCH conformer with an adjacent *trans*-diaxial H^4/Cl^5 pair, as γ-PCCH-1 presented in Scheme 1. It can be considered as a product of the conformational transition of γ-PCCH. Therefore, the transformation pathways from γ-PCCH to 1,3,4,6-TCDN via γ-PCCH-1 must be at work, in which the LinA-catalyzed dehydrochlorination reaction occurs after the conformational transition of γ-PCCH instead of eliminating the H^4/Cl^5 pair in γ-PCCH directly.

Although the LinA-catalyzed degradation process of γ-HCH have been established roughly (*4,22*), the in-depth understanding of its dehydrochlorination reaction still remains indistinct. The transition states and some intermediates as well as some products formed in the catalytic process are impossible to be observed in the general experimental enzyme chemistry, for instance, 1,3,4,6-TCDN, a very short-lived metabolism product, has never been directly detected in experimental characterization (*20*). Furthermore, the influence of residues Leu21, Ile109, and Thr133 as well as other key residues surrounding the active site of LinA in the γ-HCH dehydrochlorination process is still unknown. Therefore, theoretical calculation can be an alternative. In the present work, the detailed degradation mechanism from γ-HCH to 1,3,4,6-TCDN catalyzed by dehydrochlorinase LinA from *Sphingomonas paucimobilis* UT26 was investigated by theoretical calculations. The enzymatic step was studied with the aid of a combined quantum mechanics/molecular mechanics (QM/MM) method. QM/MM computations of the enzyme-catalyzed reaction can

provide the atomistic details of the enzyme mechanism and is therefore becoming an increasingly important tool to supplement experimental enzyme chemistry.

2. Calculation Methods

2.1 System Setup and Molecular Dynamics

The initial enzyme model for the present simulation was built on the basis of the X-ray crystal structure of γ-hexachlorocyclohexane dehydrochlorinase LinA from *Sphingomonas paucimobilis* UT26 (PDB code: 3A76) obtained from the Protein Data Bank (www.rcsb.org) (*17*). It reveals that LinA is a homotrimer with no significant difference in backbone conformation among the three chains and the LinA-catalyzed reaction can be achieved in any chain independently (*17*). Therefore, chain A of LinA was selected as the initial enzyme model for our present study. The protonation state of ionizable residues was determined on the basis of the pK_a values obtained from the PROPKA procedure (*23*). Missing hydrogen atoms of the crystal structure were supplemented through CHARMM22 force field (*24*) in the HBUILD facility of CHARMM package (*25-27*). MolProbity software was used to check the fipped Asn/Gln/His residues (*28*). Substrate models (γ-HCH and γ-PCCH-1) were built by using the Material Studio 4.4 program and then docked with the dehydrochlorinase LinA through a grid-based receptor-flexible docking module (CDOCKER) installed in the Discovery Studio 2.1 program (*29-30*) (Accelrys Software Inc.). The binding site was defined as a sphere with a radius of 5.0 Å

(coordinate: -9.806, 22.269, -5.274). Substrates were docked into the binding site with the aid of a CHARMM-based molecular dynamics (MD). Random substrate conformations were generated through high-temperature MD and translated into the binding site. Candidate poses were then created using rigid-body rotations followed by simulated annealing. A final minimization was used to refine the substrate poses. Finally, the substrate poses with interaction energy of 23.7 kcal/mol for γ-HCH and 22.8 kcal/mol for γ-PCCH-1 were select for our present work. The substrate-LinA binary complex was placed in a water sphere (TIP3P model (*31*)) with a diameter of 70.0 Å, which ensures that the complex was completely solvated. Water molecules overlapping within 2.5 Å of the binary complex were deleted. The whole system was neutralized with seven sodium ions at random positions. After that, the system was heated gradually from 0 K to 298.15 K within 50 ps and a trajectory of 500 ps was calculated to reach the thermal equilibration state (1 fs/step). Finally, a 6 ns stochastic boundary molecular dynamic (SBMD) simulation with canonical ensemble (NVT, 298.15 K) was performed to mimic the aqueous environment (*32*). The leap-frog algorithm and Langevin dynamics attached in the CHARMM package were applied during the simulation.

2.2 QM/MM Calculations

The QM/MM calculations were performed with the aid of ChemShell 3.3.01 (*33*) integrating Turbomole 6.2 (*34*) and DL-POLY (*35*) programs. The hybrid

delocalized internal coordinate (HDLC) (*36*) was adopted for the calculation. The MM region was treated with the CHARMM22 force field (*24*), while the QM region was calculated by the DFT (*37*) method. The boundary was defined by cleaving the covalent bonds between the QM and MM regions. In order to avoid over-polarization of the QM density in the QM region, hydrogen-link atoms were complemented to the QM side with the charge shift model (*38*). When partitioning the QM region, some essential criteria should be considered, residues participating in bond formation or cleavage and having strong interaction with the reactive center should be classified to the QM region. Therefore, the QM region of the LinA-catalyzed dehydrochlorination reaction system in the present study contains residues Lys20, Asp25, Trp42, His73, Arg129 and the substrate (γ-HCH or γ-PCCH-1). Together with five hydrogen-link atoms, a total of 83 atoms were treated in the QM region. Similarly, 81 atoms were regarded as QM atoms in the γ-PCCH-1 reaction system. For both of the two systems, all the atoms within 18 Å of N^{ε} atom (Scheme 1) from His73 were selected to be the active region (about 3400 movable atoms). Atoms that lie beyond 18 Å of N^{ε} were fixed during the QM/MM calculation. The QM region was optimized by the B3LYP/6-31G(d,p) method with a charge of 1 and a spin multiplicity of 1. The transition state structure was determined by scanning the potential energy profile from the reactant to the product. The corresponding structure with the highest energy along the reaction path was selected and further optimized through microiterative TS optimizer which was supported by partitioned rational function optimizer (P-RFO) algorithm (*39*) and the low-memory Broyden-Fletcher-Goldfarb-Shanno (L-BFGS)

algorithm (*40*). The character of the transition state was validated by analysis of harmonic vibrational frequencies at the B3LYP/6-31G(d,p)//CHARMM22 level. A larger basis set, B3LYP/6-311++G(d.p), was adopted in single point energy calculation. Further details of the QM/MM setup can be found in Supporting Information. In addition, the conformational transition of γ-PCCH was studied by the DFT method with solvation effect which was performed by the polarizable continuum model (PCM) (*41*) of the self-consistent reaction field theory. This method is implemented in the Gaussian09 package (*42*). Water was selected as the solvent (ε=80.0) and the PCM cavity was defined by using the default (UFF) radii. The single point energy was calculated on the basis of the B3LYP/6-31G(d,p) optimized geometries at the B3LYP/6-311++G(d,p) level of theory so that the energetic results of whole degradation process can be obtained on the same scale.

3. Results and Discussion

The LinA-substrate binary complex was extracted per picosecond during the 6,000 picosecond SBMD simulation. The corresponding root-mean-square deviations (RMSD) of the backbone for the two enzymatic reaction systems were checked and displayed in Figure S1 of the Supporting Information. Moreover, two distance variations, O^{α}-H^{β} and N^{ε}-H (N^{ε}-H^{1} for γ-HCH reaction system and N^{ε}-H^{4} for γ-PCCH-1 reaction system, the superscript can be consulted in Scheme 1), along the 6,000 picosecond trajectory were depicted in Figure S1C and D. The distance of

N^{ε}-H^{1} became stable after 1,700 picosecond of the SBMD simulation and the average distance of N^{ε}-H^{1} and N^{ε}-H^{4} were 2.75 and 2.70 Å, respectively. It can be concluded that the systems have been stabilized and the substrates meet the condition of dehydrochlorination. The distance between O^{α} and H^{β} is about 1.70 Å for both of two systems, which indicates that a hydrogen bond is formed in the catalytic dyad of LinA.

For more details to identify the reliability of the model used in our present work, three dimensional models for the docked structures, MD snapshots, and QM/MM-optimised structures were exhibited in Supporting Information. For the γ-HCH reaction system (Figure S2), the substrate keeps its chair conformation with the position staying relatively stationary in the three sections. The relative position with His73 is measured through distance of N^{ε}-H^{1}, which is 2.63 Å in docked structure, an average of 2.75 Å in MD snapshots, and an average of 2.46 Å in QM/MM-optimised structures. Similarly, D1, D2 and D3 are also adopted to estimate the relative position with Trp42, Arg129 and Lys20, which are about 3.50 Å, 5.00 Å and 4.90 Å in the three sections. Analogously, the half-chair conformation γ-PCCH-1 (Figure S3) is also located in the active site with a relatively stable position. Hence, it might be inferred that the model used in our present work could be credible for the present study.

3.1 Reaction Mechanism and Energetic Results

The rate constant of an enzyme-catalyzed reaction generally exhibits a

223 wide range of fluctuation instead of a constant, according to the room-temperature
224 single molecule experiment (*43-44*). It is assumed that each snapshot extracted from
225 the dynamics trajectory corresponds to a local rate constant (*45*). The potential barrier
226 of an enzymatic reaction is supposed to be a statistic value by considering all the
227 fluctuant results. In order to obtain the potential barrier of an enzymatic reaction, the
228 Boltzmann-weighted averaging method is introduced. It can be described by the
229 following equation (*46-47*):

230 $$\Delta E_{ea} = -RT \ln\left\{\frac{1}{n}\sum_{i=1}^{n}\exp\left(\frac{-\Delta E_i}{RT}\right)\right\}$$

231 Where, ΔE_{ea} is the Boltzmann-weighted average potential barrier, R is gas constant, T
232 is the temperature, n is the number of snapshots, and ΔE_i is the potential barrier of
233 pathway i. In the present study, five different snapshots were extracted every 0.5 ns
234 from 4 to 6 ns from the SBMD simulations. They were labeled as SH-4.0, SH-4.5,
235 SH-5.0, SH-5.5, and SH-6.0 for the γ-HCH dehydrochlorination reaction system and
236 SP-4.0, SP-4.5, SP-5.0, SP-5.5, and SP-6.0 for the γ-PCCH-1 dehydrochlorination
237 reaction system. These structures served as the starting configurations in the following
238 geometry optimization and transition-state search.

239 The degradation process of γ-HCH covers three elementary steps:
240 dehydrochlorination of γ-HCH, conformational transition of γ-PCCH, and
241 dehydrochlorination of γ-PCCH-1, as indicated in Scheme 1A. Energy profiles of the
242 three steps are calculated and shown in Figure 1. For the dehydrochlorination of
243 γ-HCH, a substantial potential barrier spread from 12.6 to 21.3 kcal/mol is found
244 among different snapshots as listed in Table 1. The large potential barrier fluctuation

observed is helpful in understanding the room-temperature single molecule experimental evidence that the reaction rate of a single enzyme molecule exhibits large fluctuation (*43-44*). The calculated average potential barrier for dehydrochlorination of γ-HCH, 16.2 kcal/mol, conforms exactly to the experimental result of ~16 kcal/mol, which is converted from experimentally determined k_{cat} value (63.5 s^{-1} (*48*)) with the aid of the conventional transition-state theory (*49*). Similarly, a potential barrier fluctuation spread from 13.4 to 21.5 kcal/mol listed in Table 2 is found in the second dehydrochlorination step (dehydrochlorination of γ-PCCH-1) and the calculated average potential barrier is 17.3 kcal/mol, a slightly higher than that of the dehydrochlorination of γ-HCH. For the conformational transition of γ-PCCH, the calculated potential barrier is 11.1 kcal/mol. It is worth noticing that all of the three elementary steps are exothermic, the enthalpy of reaction (ΔH, 298.15 K) is -4.7 kcal/mol for dehydrochlorination of γ-HCH, -1.0 kcal/mol for conformational transition of γ-PCCH and -19.3 kcal/mol for dehydrochlorination of γ-PCCH-1. The low potential barrier and strong exothermicity of three elementary steps indicate that they are energetically feasible. Consequently, the assumed metabolic pathway from γ-HCH to 1,3,4,6-TCDN catalyzed by dehydrochlorinase LinA from *Sphingomonas paucimobilis* UT26 is reasonable.

3.2 Catalytic Itinerary and Structural Details

For convenience of description, several key atoms in the QM region are

numbered for the LinA-catalyzed dehydrochlorination of γ-HCH, as presented in Scheme 1B. Some crucial internuclear distances in the reactant, transition state, and product computed at the B3LYP/6-31G(d,p)//CHARMM22 level are provided in Table 1. Since a majority of the catalytic reactions occur through the pathway with the lowest potential barrier, the following investigation towards γ-HCH dehydrochlorination process will mainly focus on the pathway SH-5.5. For a more intuitive observation, the three dimensional structures of R, TS-1, and IM-1 involved in the γ-HCH dehydrochlorination step of the pathway SH-5.5 are displayed in Figure 2. Obviously, an adjacent *trans*-diaxial H/Cl pair composed by H^1 and Cl^2 is situated towards the N^{ε} atom of His73 residue in the reactant, and the distance between H^1 and N^{ε} is 2.58 Å. It reveals that the γ-HCH molecule satisfies the condition of dehydrochlorination by LinA. In the process from the reactant to the transition state, the bond length of C^1-H^1 is stretched from 1.09 Å to 1.53 Å and the distance between N^{ε} and H^1 is reduced to 1.24 Å, indicating that H^1 is delivered from γ-HCH to His73 residue. The character of the transition state is verified by the vibrational mode and the corresponding imaginary frequency of 770i cm^{-1}. In the product, the length of double bond C^1=C^2 (1.33 Å) and the angles of Cl^1-C^1-C^2 (118.9°), H^2-C^2-C^1 (120.4°) as well as the dihedral angle of H^1-C^1-C^2-Cl^2 (0.8°) suggest the formation of γ-PCCH. Meanwhile, the distance of C^2-Cl^2 (2.97 Å) suggests the formation of a chloride anion. The new-formed chloride anion can be stabilized by a positively charged region constituted by Lys20 and Arg129. It is compelling to note that the hydrogen bond between O^{α} and H^{β} becomes stronger during the process of proton H^1 transferring

289 from γ-HCH to His73 residue. Hence, Asp25 can distribute the positive charge in
290 protonated imidazole ring of His73.

291 For a more detailed description, the internuclear distance and Mulliken
292 population analysis charge variations are introduced. Figure 3A shows the variations
293 of four crucial internuclear distances along the γ-HCH dehydrochlorination process. It
294 is evident that the dehydrogenation and dechlorination process occur simultaneously,
295 theoretically confirming the fact that LinA catalyzes degradation of γ-HCH via an E2
296 mechanism. The atomic charge analysis of several key atoms is displayed in Figure
297 3B. The negative charge of N^{ε} has been weakened along the process, corresponding to
298 the state of proton transfer. The anion character of Cl^2 in the product was further
299 confirmed by its negative charge (-0.48).

300 The intermediate γ-PCCH will diffuse out of the enzyme when the
301 dehydrochlorination of γ-HCH is completed (*17*). As a consequence, the subsequent
302 conformational transition of γ-PCCH is nonenzymatic. In the present work, the
303 conformational transition step was considered by the DFT method with solvation
304 effect. The structures of reactant, transition state and product optimized at the
305 B3LYP/6-31G(d,p) level are exhibited in Figure 1. During the conformational
306 transition process, the dihedral angle of C^3-C^4-C^5-C^6 varies from -58.8° to 59.9°,
307 indicates that the relative position of C^4 and C^5 has been inverted. The adjacent
308 diequatorial H^4/Cl^5 pair is converted to *trans*-diaxial H^4/Cl^5 pair. The transformation
309 from one half-chair conformer (γ-PCCH) to another half-chair conformer (γ-PCCH-1)
310 is accomplished. It is worth noting that the dihedral angle of C^3-C^4-C^5-C^6 in transition

state is approximately 0°, suggests this four carbon atoms are coplanar in the cyclohexene structure. However, all the six carbon atoms of the cyclohexene structure are not situated in the same plane. The dihedral angle of C^1-C^2-C^3-C^4 (33.7°) and C^2-C^1-C^6-C^5 (-33.2°) reveals that the transition state is a boat form structure. The character of the transition state is also verified by the vibrational mode and the corresponding imaginary frequency of 54i cm^{-1}.

For the dehydrochlorination of γ-PCCH-1, some crucial QM atoms are numbered in Scheme 1C. The degradation process was investigated at the B3LYP/6-31G(d,p)//CHARMM22 level. Four selected internuclear distances in the reactant, transition state and product are provided in Table 2 respectively. Figure 4 displays the active site structures of IM-2, TS-3, and P in the pathway SP-6.0 as it executes the dehydrochlorination process with the lowest potential barrier. An overall view of the reaction process indicates that the dehydrochlorination of γ-PCCH-1 is accomplished with the same mechanism as that from γ-HCH. The metabolism product 1,3,4,6-TCDN is optimized successfully, theoretically verifying the existence of the putative short-lived product. The distance between the leaving chlorine atom (Cl^5) and its interrelated carbon atom (C^5) is 3.78 Å. However, the negative charge of the leaving chlorine atom Cl^5 (-0.29) is incomprehensibly weaker than that of Cl^2 (-0.48). A reasonable explanation is that the chloride anion Cl^5 is closer to the positively charged region constituted by Lys20 and Arg129, causing a more sufficient charge dispersion.

3.3 Individual Residue Influence

According to previous crystal structure study, the active site of LinA is largely surrounded by fourteen residues (*17*). They can make an electrostatic influence on the enzyme reaction, though they do not participate in the reaction directly. In order to clarify the electrostatic influence of the residues surrounding the active site, the electrostatic interaction energies of the fourteen residues were estimated towards the two dehydrochlorination processes. The electrostatic influence of an amino acid i can be described as:

$$\Delta E^{i-0} = \Delta E^{i} - \Delta E^{0}$$

Where, ΔE^{i-0} is the changes of the barrier, ΔE^{i} is the potential barrier with charges on residue i set to 0, and ΔE^{0} is the original values of the potential barrier. During all these energy calculations, the geometry structures of the stationary points were kept unchanged. A positive ΔE^{i-0} value means that neglecting the influence of the i^{th} residue will increase the potential barrier. In other words, the i^{th} residue can diminish the potential barrier and facilitate the enzyme reaction. Contrarily, a negative ΔE^{i-0} value denotes that the i^{th} residue can increase the potential barrier and suppress the enzyme reaction (*47*).

The ΔE^{i-0} values of fourteen residues studied in the current work were schematically described in Figure 5. For the dehydrochlorination of γ-HCH, the electrostatic influence analysis shows that residue Phe68 facilitates this degradation reaction ($\Delta E^{i-0} > 1$ kcal/mol), whereas residues Leu21 and Cys71 suppress it ($\Delta E^{i-0} <$

-1 kcal/mol). The other eleven residues are found to perform a negligible influence (-1 kcal/mol $< \Delta E^{i-0} <$ 1 kcal/mol) towards the dehydrochlorination of γ-HCH. This electrostatic influence analysis highlights Leu21 and Cys71 as candidate residues for future mutation studies. In addition, all the fourteen residues studied in this analysis are found to have a weaker effect (-1 kcal/mol $< \Delta E^{i-0} <$ 1 kcal/mol) on the dehydrochlorination of γ-PCCH-1.

4. Conclusions

The present work investigated the biotransformation pathway from γ-HCH to 1,3,4,6-TCDN catabolized by dehydrochlorinase LinA from *Sphingomonas paucimobilis* UT26. The degradation process contains two discontinuous dehydrochlorination reactions. The product of the first dehydrochlorination step undergoes a conformational transition instead of executing the second dehydrochlorination step directly. The electrostatic influence analysis reveals that the residue Phe68 facilitates the degradation reaction most and the residues Leu21 and Cys71 suppress it. It can be a valuable base for rational design of mutants of dehydrochlorinase LinA with a more efficient activity towards the degradation of γ-HCH and further experimental verification would be anticipated.

Acknowledgments

This work was supported by NSFC (National Natural Science Foundation of China, project Nos. 21337001, 21177077) and the Research Fund for the Doctoral Program of Higher Education of China (project No. 20130131110058).

Supplementary data

Root-mean-square deviations (RMSD) of the backbone and key distance variations along the molecular dynamic simulations (Figure S1); the three dimensional structures of the docked structure, the MD snapshot, and the QM/MM-optimised structure in the γ-HCH and γ-PCCH-1 reaction systems (Figure S2 and Figure S3); additional details on the methods; the coordinates of the docked structures, MD snapshots, QM-optimized structures and QM/MM-optimized structures.

References

1 V. Raina, A. Hauser, H. R. Buser, D. Rentsch, P. Sharma, R. Lal, C. Holliger, T. Poiger, M. D. Muller and H. P. E. Kohler, *Environ. Sci. Technol.*, 2007, **41**, 4292-4298.

2 M. Okai, J. Ohtsuka, L. F. Imai, T. Mase, R. Moriuchi, M. Tsuda, K. Nagata, Y. Nagata and M. Tanokura, *J. Bacteriol.*, 2013, **195**, 2642-2651.

3 K. L. Willett, E. M. Ulrich and R. A. Hites, *Environ. Sci. Technol.*, 1998, **32**, 2197-2207.

4 R. Lal, G. Pandey, P. Sharma, K. Kumari, S. Malhotra, R. Pandey, V. Raina, H. P. E. Kohler, C. Holliger, C. Jackson and J. G. Oakeshott, *Microbiol. Mol. Biol. Rev.*, 2010, **74**, 58-80.

5 M. Suar, A. Hauser, T. Poiger, H. R. Buser, M. D. Müller, C. Dogra, V. Raina, C. Holliger, J. R. van der Meer and R. Lal, *Appl. Environ. Microbiol.*, 2005, **71**, 8514-8518.

6 K. Bala, B. Geueke, M. Miska, D. Rentsch, T. Poiger, M. Dadhwal, R. Lal, C. Holliger and H. P. E. Kohler, *Environ. Sci. Technol.*, 2012, **46**, 4051-4058.

7 K. Walker, D. A. Vallero and R. G. Lewis, *Environ. Sci. Technol.*, 1999, **33**, 4373-4378.

8 H. R. Buser and M. D. Muller, *Environ. Sci. Technol.*, 1995, **29**, 664-672.

9 P. J. Middeldorp, W. van Doesburg, G. Schraa and A. J. Stams, *Biodegradation*, 2005, **16**, 283-290.

10 T. M. Phillips, A. G. Seech, H. Lee and J. T. Trevors, *Biodegradation*, 2005, **16**,

363-392.

11 S. Nagasawa, R. Kikuchi, Y. Nagata, M. Takagi and M. Matsuo, *Chemosphere*, 1993, **26**, 1719-1728.

12 H. H. M. Rijnaarts, A. Bachmann, J. C. Jumelet and A. J. B. Zehnder, *Environ. Sci. Technol.*, 1990, **24**, 1349-1354.

13 S. K. Sahu, K. K. Patnaik, S. Bhuyan, B. Sreedharan, N. Kurihara, T. K. Adhya and N. Sethunathan, *J. Agric. Food Chem.*, 1995, **43**, 833-837.

14 S. K. Sahu, K. K. Patnaik and N. Sethunathan, *Bull. Environ. Contam. Toxicol.*, 1992, **48**, 265-268.

15 S. K. Sahu, K. K. Patnaik, M. Sharmila and N. Sethunathan, *Appl. Environ. Microbiol*., 1990, **56**, 3620-3622.

16 D. Boltner, S. Moreno-Morillas and J. L. Ramos, *Environ. Microbiol.*, 2005, **7**, 1329-1338.

17 M. Okai, K. Kubota, M. Fukuda, Y. Nagata, K. Nagata and M. Tanokura, *J. Mol. Biol.*, 2010, **403**, 260-269.

18 Y. Nagata, K. Miyauchi and M. Takagi, *J. Ind. Microbiol. Biotechnol.*, 1999, **23**, 380-390.

19 R. Imai, Y. Nagata, M. Fukuda, M. Takagi and K. Yano, *J. Bacteriol.*, 1991, **173**, 6811-6819.

20 L. Trantírek, K. Hynkova, Y. Nagata, A. Murzin, A. Ansorgova, V. Sklenaŕ and J. Damborsky, *J. Biol. Chem.*, 2001, **276**, 7734-7740.

21 P. G. Deo, N. G. Karanth and N. G. Karanth, *Crit. Rev. Microbiol*., 1994, **20**,

57-78.

22 R. Lal, M. Dadhwal, K. Kumari, P. Sharma, A. Singh, H. Kumari, S. Jit, S. K. Gupta, D. Lal, M. Verma, J. Kaur, K. Bala and S. Jindal, *Indian J. Microbiol.*, 2008, **48**, 3-18.

23 H. Li, A. D. Robertson and J. H. Jensen, *Proteins*, **2005**, **61**, 704-721.

24 A. D. MacKerell, D. Bashford, M. Bellott, R. L. Dunbrack, J. D. Evanseck, M. J. Field, J. Gao, H. Guo, S. Ha, D. Joseph-McCarthy, L. Kuchnir, K. Kuczera, F. T. Lau, C. Mattos, S. Michnick, T. Ngo, D. T. Nguyen, B. Prodhom, W. E. Reiher, B. Roux III, M. Schlenkrich, J. C. Smith, R. Stote, J. Straub, M. Watanabe, J. Wiórkiewicz-Kuczera, D. Yin and M. Karplus, *J. Phys. Chem. B*, 1998, **102**, 3586-3616.

25 B. R. Brooks, R. E. Bruccoleri, B. D. Olafson, D. J. States, S. Swaminathan and M. Karplus, *J. Comput. Chem.*, 1983, **4**, 187-217.

26 B. R. Brooks, C. L. Brooks III, A. D. Mackerell, L. Nilsson, R. J. Petrella, B. Roux, Y. Won, G. Archontis, C. Bartels, S. Boresch, A. Caflisch, L. Caves, Q. Cui, A. R. Dinner, M. Feig, S. Fischer, J. Gao, M. Hodoscek, W. Im, K. Kuczera, T. Lazaridis, J. Ma, V. Ovchinnikov, E. Paci, R. W. Pastor, C. B. Post, J. Z. Pu, M. Schaefer, B. Tidor, R. M. Venable, H. L. Woodcock, X. Wu, W. Yang, D. M. York and M. Karplus, *J. Comput. Chem*., 2009, **30**, 1545-1615.

27 A. D. MacKerell Jr, B. Brooks, C. L. Brooks III, L. Nilsson, B. Roux, Y. Won and M. Karplus, *Encyclopedia Comput. Chem.*, 1998, **1**, 271-277.

28 V. B. Chen, W. B. Arendall III, J. J. Headd, D. A. Keedy, R. M. Immormino, G. J.

Kapral, L. W. Murray, J. S. Richardson and D. C. Richardson, *Acta Crystallogr., Sect. D: Biol. Crystallogr.*, 2010, **66**, 12-21.

29 G. Wu, D. H. Robertson, C. L. 3rd. Brooks and M. Vieth, *J. Comput. Chem.*, 2003, **24**, 1549-1562.

30 M. Vieth, J. D. Hirst, A. Kolinski and C. L. 3rd. Brooks, *J. Comput. Chem.*, 1998, **19**, 1612-1622.

31 W. L. Jorgensen, J. Chandrasekhar, J. D. Madura, R. W. Impey and M. L. Klein, *J. Chem. Phys*., 1983, **79**, 926-935.

32 C. L. Brooks and M. Karplus, *J. Chem. Phys.*, 1983, **79**, 6312-6325.

33 P. Sherwood, A. H. D. Vries, M. F. Guest, G. Schreckenbach, C. R. A. Catlow, S. A. French, A. A. Sokol, S. T. Bromley, W. Thiel, A. J. Turner, S. Billeter, F. Terstegen, S. Thiel, J. Kendrick, S. C. Rogers, J. Casci, M. Watson, F. King, E. Karlsen, M. Sjovoll, A. Fahmi, A. Schafer and C. Lennartz, *J. Mol. Struct.: THEOCHEM*, 2003, **632**, 1-28.

34 R. Ahlrichs, M. Bär, M. Häser, H. Horn and C. Kölmel, *Chem. Phys. Lett.*, 1989, **162**, 165-169.

35 W. Smith and T. R. Forester, *J. Mol. Graphics Modell.*, 1996, **14**, 136-141

36 S. R. Billeter, A. J. Turner and W. Thiel, *Phys. Chem. Chem. Phys.*, 2000, **2**, 2177-2186.

37 K. Burke, J. Werschnik and E. K. U. Gross, *J. Chem. Phys.*, 2005, **123**, 1-9.

38 A. H. de Vries, P. Sherwood, S. J. Collins, A. M. Rigby, M. Rigutto and G. J. Kramer, *J. Phys. Chem. B*, 1999, **103**, 6133-6141.

39 J. Baker, *J. Comput. Chem.*, 1986, **7**, 385-395.

40 D. C. Liu and J. Nocedal, *Math. Program.*, 1989, **45**, 503-528.

41 C. Amovilli, V. Barone, R. Cammi, E. Cances, M. Cossi, B. Mennucci, C. S. Pomelli and J. Tomasi, *Adv. Quantum Chem.*, 1998, **32**, 227-261.

42 M. J. Frisch, G. W. Trucks, H. B. Schlegel, P. W. M. Gill, B. G. Johnson, M. A. Robb, J. R. Cheeseman, T. A. Keith, G. A. Petersson and J. A. Montgomery, GAUSSIAN 03, Pittsburgh, PA, 2003.

43 H. P. Lu, L. Y. Xun and X. S. Xie, *Science*, 1998, **282**, 1877-1882.

44 W. Min, B. P. English, G. Luo, B. J. Cherayil, S. C. Kou and X. S. Xie, *Acc. Chem. Res.*, 2005, **38**, 923-931.

45 Y. W. Li, R. M. Zhang, L. K. Du, Q. Z. Zhang and W. X. Wang, *RSC Adv.*, 2015, **5**, 13871-13877.

46 R. Lonsdale, J. N. Harvey and A. J. Mulholland, *J. Phys. Chem. B*, 2010, **114**, 1156-1162.

47 Y. W. Li, X. L. Shi, Q. Z. Zhang, J. T. Hu, J. M. Chen and W. X. Wang, *Environ. Sci. Technol.*, 2014, **48**, 5008-5016.

48 D. R. B. Brittain, R. Pandey, K. Kumari, P. Sharma, G. Pandey, R. Lal, M. L. Coote, J. G. Oakeshott and C. J. Jackson, *Chem. Commun.*, 2011, **47**, 976-978.

49 J. R. Alvarez-Idaboy, A. Galano, G. Bravo-Perez and M. E. Ruiz, *J. Am. Chem. Soc.*, 2001, **123**, 8387-8395.

Table 1 Potential barriers $\Delta E^{\ddagger}$ (in kcal/mol) and enthalpy of reaction ΔH (in kcal/mol) as well as selected internuclear distances (in Å) in the reactant (R), transition state (TS-1) and product (IM-1) involved in the LinA-catalyzed dehydrochlorination of γ-HCH in five pathways. ΔH is calculated at 298.15 K.

pathway	N^{ε}-H^1			H^1-C^1			C^1-C^2			C^2-Cl^2			$\Delta E^{\ddagger}$	ΔH
	R	TS-1	IM-1	R	TS-1	IM-1	R	TS-1	IM-1	R	TS-1	IM-1		
SH-4.0	2.42	1.23	1.02	1.09	1.57	2.60	1.53	1.48	1.34	1.82	1.95	2.91	12.6	-3.9
SH-4.5	2.41	1.23	1.01	1.09	1.55	2.97	1.53	1.48	1.33	1.83	1.96	2.97	17.4	-5.4
SH-5.0	2.37	1.21	1.01	1.09	1.57	2.60	1.53	1.48	1.33	1.82	1.93	2.92	16.8	-0.2
SH-5.5	2.58	1.24	1.01	1.09	1.53	2.61	1.52	1.48	1.33	1.82	1.93	2.97	12.8	-9.1
SH-6.0	2.53	1.22	1.01	1.09	1.56	2.78	1.53	1.48	1.33	1.82	1.94	3.16	21.3	-4.9

Table 2 Potential barriers $\Delta E^{\ddagger}$ (in kcal/mol) and enthalpy of reaction ΔH (in kcal/mol) as well as selected internuclear distances in the reactant (IM-2), transition state (TS-3) and product (P) involved in the LinA-catalyzed dehydrochlorination of γ-PCCH-1 in five pathways. ΔH is calculated at 298.15 K.

pathway	N^{ε}-H^4			H^4-C^4			C^4-C^5			C^5-Cl^5			$\Delta E^{\ddagger}$	ΔH
	IM-2	TS-3	P	IM-2	TS-3	P	IM-2	TS-3	P	IM-2	TS-3	P		
SP-4.0	2.40	1.25	1.01	1.10	1.52	2.97	1.53	1.49	1.33	1.82	1.90	4.15	14.9	-19.8
SP-4.5	2.41	1.20	1.01	1.09	1.60	3.15	1.52	1.49	1.34	1.82	1.90	4.01	21.5	-22.8
SP-5.0	2.50	1.25	1.01	1.09	1.52	3.03	1.53	1.50	1.33	1.82	1.91	3.94	19.5	-18.7
SP-5.5	2.48	1.26	1.01	1.09	1.53	2.98	1.53	1.50	1.34	1.82	1.90	4.16	17.3	-16.3
SP-6.0	2.26	1.23	1.01	1.10	1.53	2.81	1.53	1.49	1.34	1.82	1.91	3.78	13.4	-18.9

Figure Captions

Scheme 1. (A) The degradation pathway from γ-HCH to 1,3,4,6-TCDN catabolized by dehydrochlorinase LinA. The leaving atoms are labeled in bold red. The QM region for LinA-catalyzed dehydrochlorination of γ-HCH (B) and γ-PCCH-1 (C). Several key atoms are numbered and the boundary between the QM and MM regions is indicated by wavy lines.

Figure 1. Energy profiles of three elementary steps along the transformation process from γ-HCH to 1,3,4,6-TCDN. The structures of the reactant (γ-PCCH), transition state (TS-2) and product (γ-PCCH-1) involved in the conformational transition step are exhibited in ball and stick models. The potential barriers of each elementary step are provided in the braces.

Figure 2. The three dimensional structures of the reactant (R), transition state (TS-1), and product (IM-1) involved in the pathway SH-5.5 of the γ-HCH dehydrochlorination step. The QM atoms including link hydrogen atoms are shown in ball and stick representation. The unit of bond distances and imaginary frequency are in Å and cm^{-1}.

Figure 3. Variations of four crucial internuclear distances (A) and atomic charges of several key atoms (B) along pathway SH-5.5 of the γ-HCH dehydrochlorination process.

Figure 4. The three dimensional structures of the reactant (IM-2), transition state (TS-3), and product (P) involved in the pathway SP-6.0 of the γ-PCCH-1

dehydrochlorination step. The QM atoms including link hydrogen atoms are shown in ball and stick representation. The unit of bond distances and imaginary frequency are in Å and cm^{-1}.

Figure 5. ΔE^{i-0} values of fourteen individual residues toward the dehydrochlorination of γ-HCH and γ-PCCH-1.

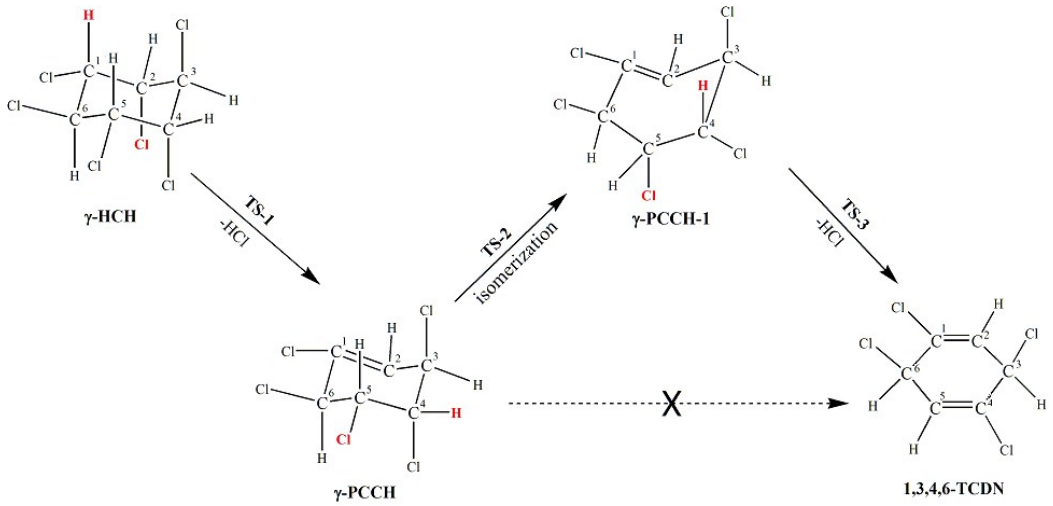

A

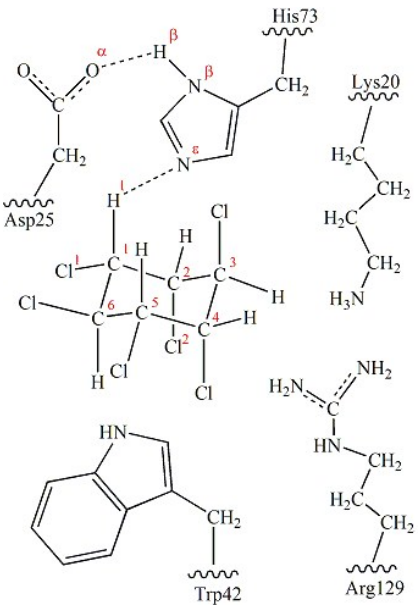

B

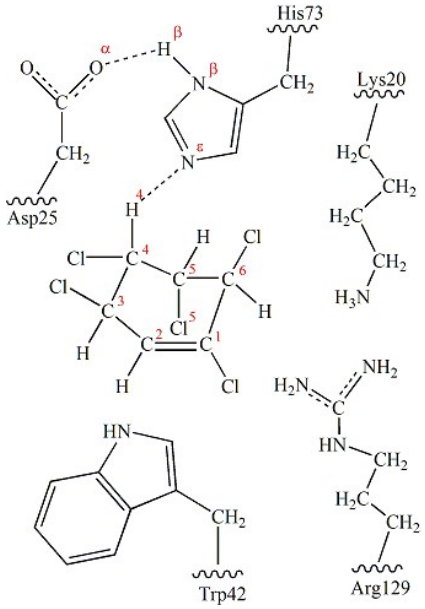

C

Scheme 1

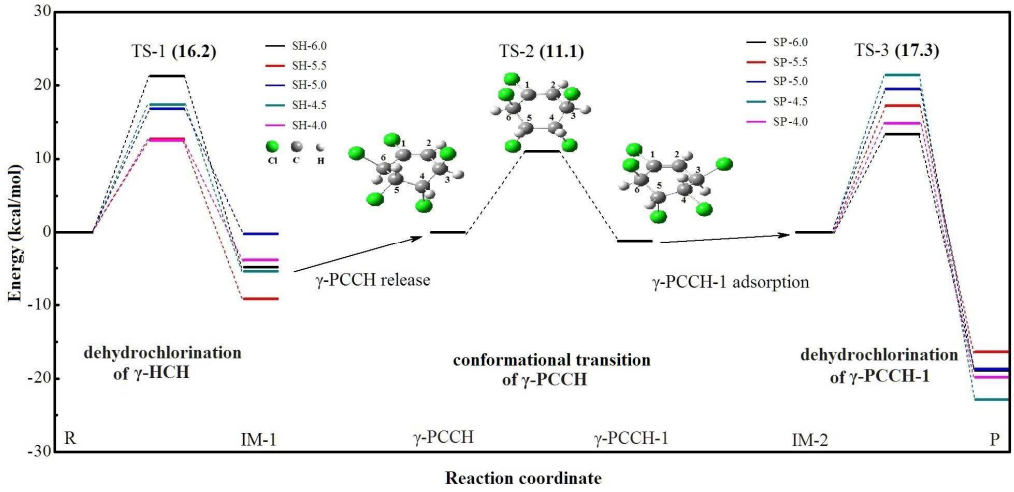

Figure 1

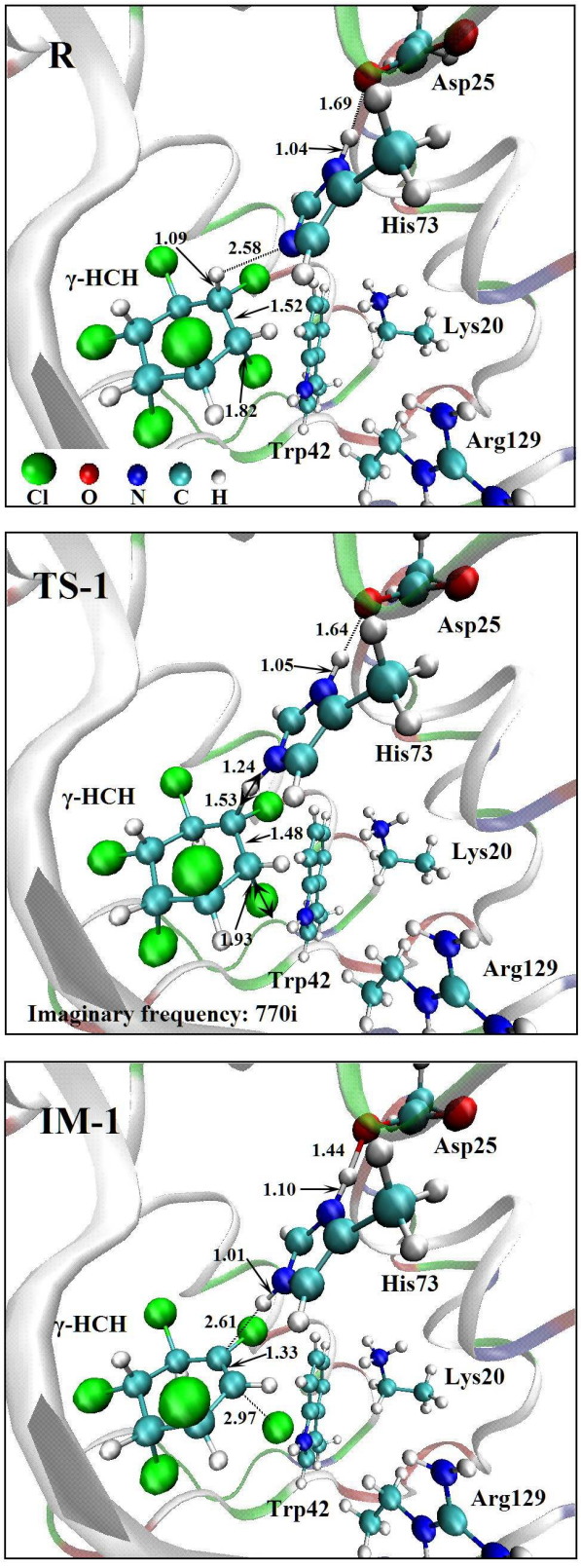

593

594 Figure 2

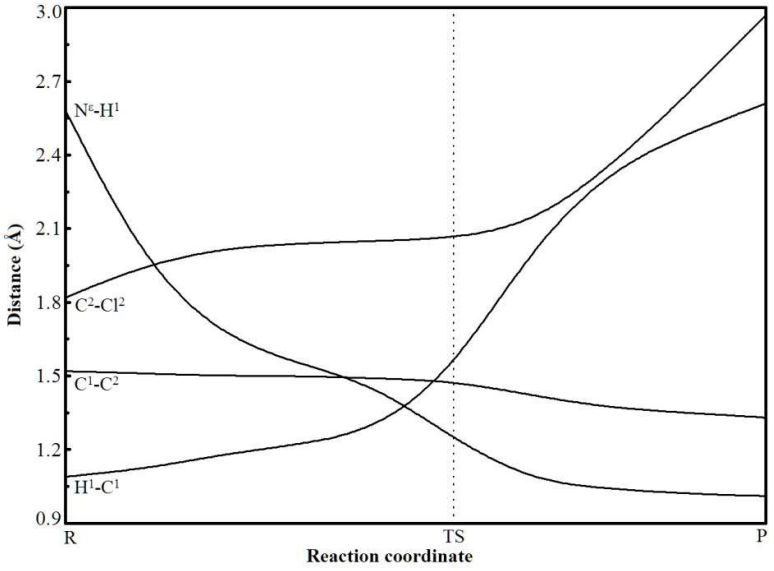

595

596 A

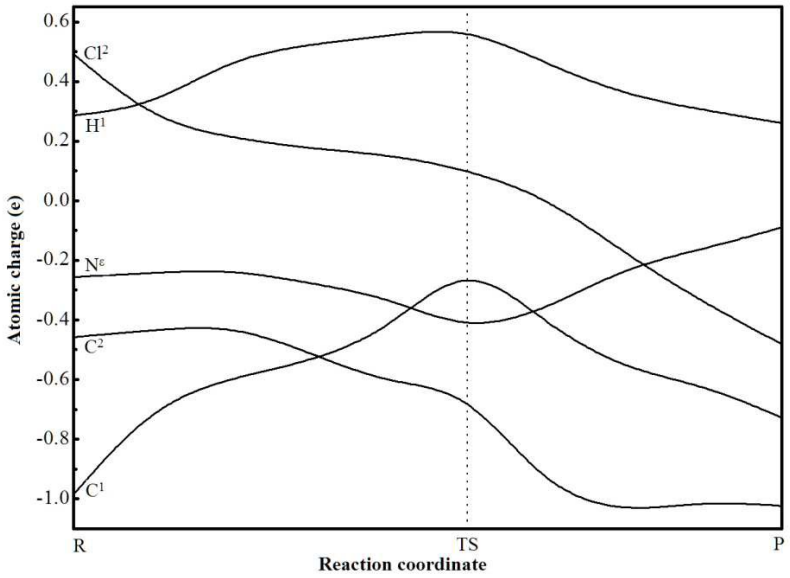

597

598 B

599

600 Figure 3

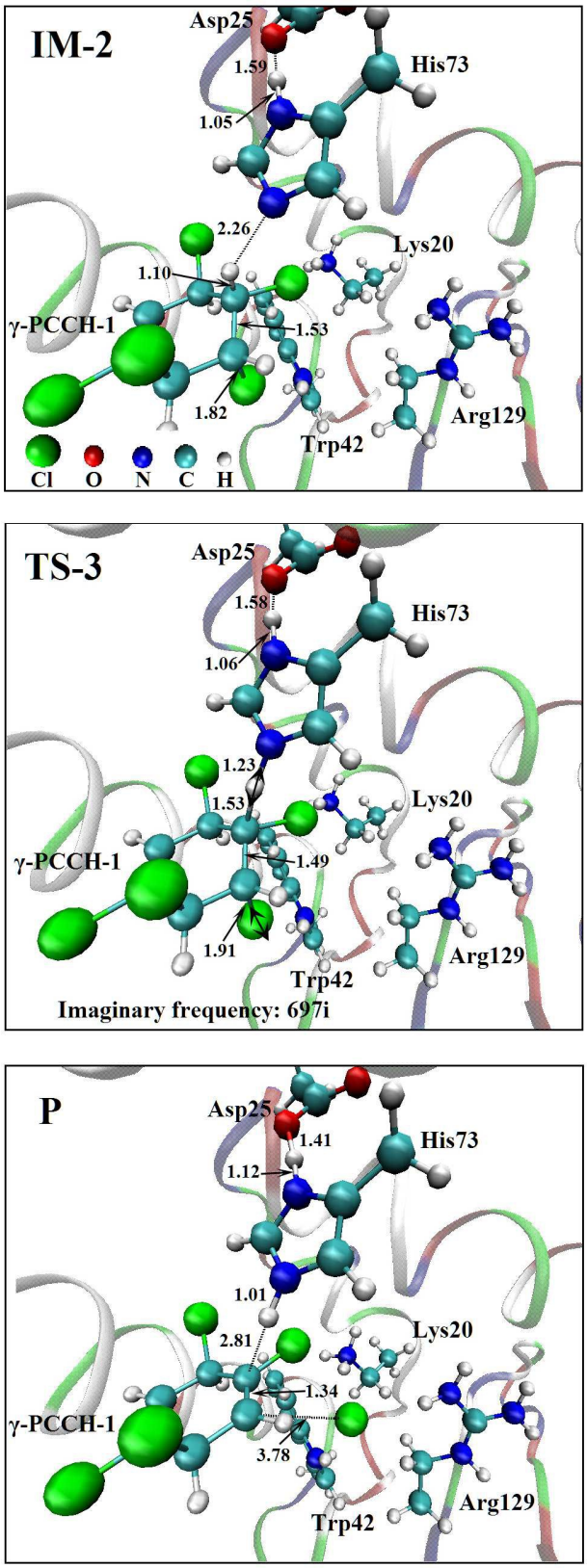

601

602 Figure 4

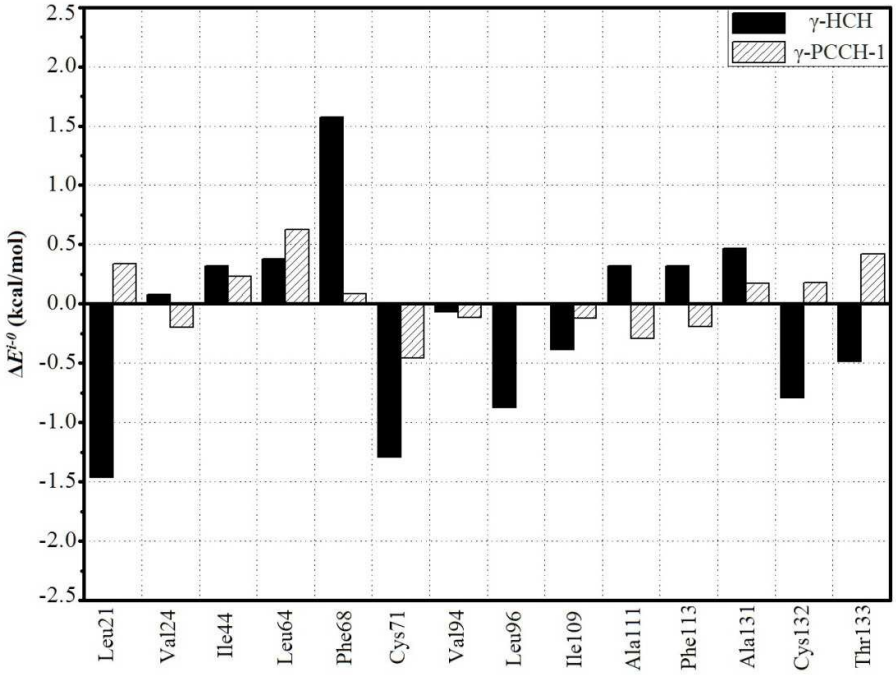

Figure 5

Graphical abstract:

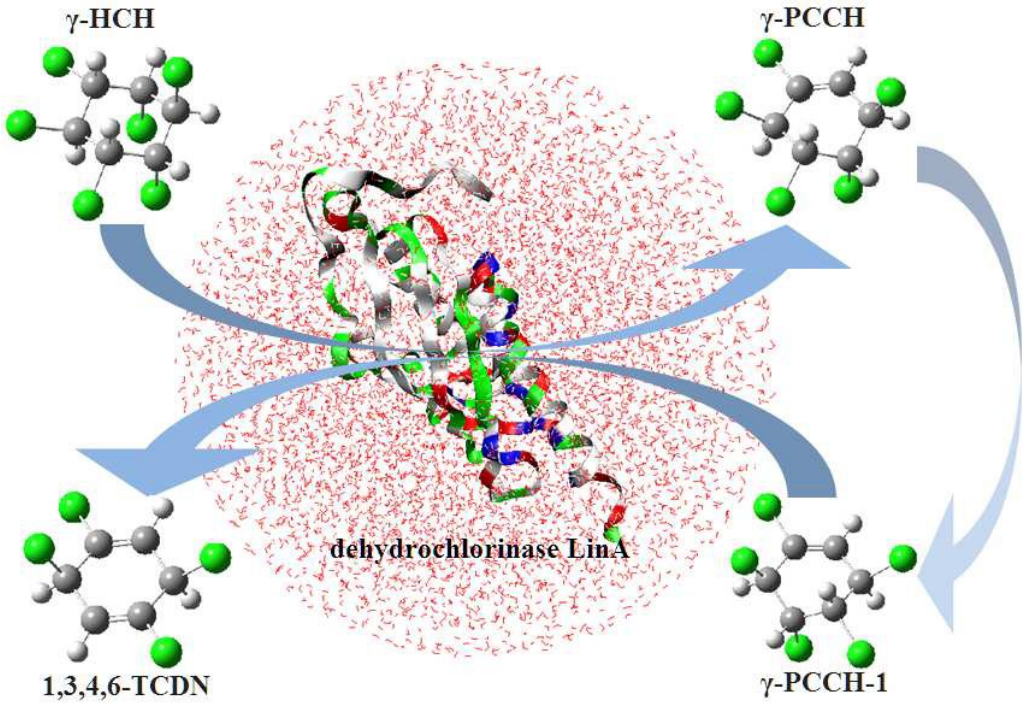

The biotransformation pathway from γ-HCH to 1,3,4,6-TCDN catabolized by dehydrochlorinase LinA contains two discontinuous dehydrochlorination reactions and the product of the first dehydrochlorination step undergoes a conformational transition instead of executing the second dehydrochlorination step directly.